Experiments on a Repetitively Pulsed Electrothermal Thruster

R. L. Burton,* D. Fleischer,† S. A. Goldstein,‡ and D. A. Tidman§
GT-Devices, Inc., Alexandria, Virginia 22312

This paper presents experimental results for a pulsed electrothermal (PET) thruster using water propellant. The PET thruster produces several hundred atmospheres pressure in a capillary-confined discharge, coupled to a supersonic, equilibrium flow nozzle. The thruster head has a ceramic capillary insulator and tungsten alloy electrodes, with water propellant injected axially from a central orifice. The thruster is repetitively driven at 2–10 pps by a capacitive pulse-forming network (PFN), with a discharge power of 3–6 MW and an average power of 80–630 W. The measured thrust-to-power ratio is $T/P = 0.07 \pm 0.01$ N/kW. Discharge conditions are inferred from a numerical model that predicts pressure and temperature levels of 300–500 atm and 20,000 K, respectively. The estimated exhaust velocity, with a test tank background pressure of 10–20 Torr, is 14 km/s, corresponding to a thrust efficiency of 54±7%.

I. Introduction

THE pulsed electrothermal (PET) thruster, essentially a high-resistance, high-pressure electrothermal discharge coupled to a supersonic nozzle, has been proposed[1] as a way to achieve high efficiency at 1000- to 2000-s specific impulse, a regime of particular interest for near-Earth missions ranging from attitude control to primary propulsion. At 1000–2000 s, propellant savings are significant in comparison to chemical thrusters, yet the thrust is high enough that thrust times are not excessive.

The major goal of PET thruster development is to provide sufficient system lifetime and efficiency (over 50%) to justify the modest increase in system complexity from dc systems. A comparison of predicted PET thruster performance for water and liquid hydrogen propellant is compared to that for competing electric thrusters in Fig. 1. It can be seen that no existing system except PET is yet a candidate for high efficiency at 1000–2000 s.

In previous work,[2,3] data were presented on a PET thruster for which the discharge pressure was contained by a solid polyethylene (C_2H_4) liner which ablated to feed polyethylene propellant to the arc. Subsequent works[4,5] refined the performance measurements for the ablating polyethylene thruster and presented a conceptual design for a PET thruster system fed by storable liquids such as water. Subsequently, preliminary experiments were conducted to verify PET thruster operation with water propellant and to measure the breakdown field strength for the device.[6]

In the present experiments,[7] the PET thruster is designed to operate with liquid propellant in a repetitive mode without a switch or a pulsed propellant valve. The thruster capacitors are allowed to charge to the breakdown voltage and then directly discharge to the thruster electrodes. This operational mode simplifies the thruster system at the expense of small shot-to-shot variations in thruster impulse.

The purpose of the present work is to demonstrate technical feasibility for the PET thruster. The goal is to operate at a mean power of several hundred watts using water propellant and to achieve significantly higher efficiencies than other electric thrusters in the 1000- to 2000-s specific impulse (I_{sp}) range. The successful results of this effort are discussed in the next section.

II. Repetitive PET Thruster Operation

The water-injected PET thruster used in this experiment (Fig. 2) operates at a multi-megawatt peak power level by discharging small amounts of energy (40–80 J) on a time scale of tens of microseconds. The water subjected to this power level is continuously injected at a mass flow of only a few milligrams per second and is heated to 15,000–25,000 K at a pressure of 20–600 atm. A thruster average power in the kilowatt range is achieved by pulsing the thruster. A maximum of 25 pps is used in these experiments, but up to 40 pps has been achieved in later experiments with improved capacitors.

Because of the high discharge pressure, flow in the nozzle is in equilibrium for most of the expansion process, and the ionization energy is completely recovered. The exhaust flow therefore consists entirely of water molecules and products of dissociation.

In order to withstand the high heat-transfer rates in the thruster, the power is supplied to the electrodes in a short

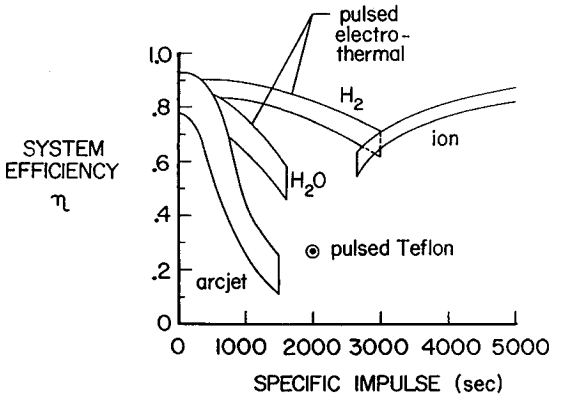

Fig. 1 Comparison of PET thruster performance with electrothermal, electromagnetic pulsed Teflon, and electrostatic ion thrusters.

Received March 9, 1987; presented as Paper 87-1043 at the 19th AIAA/DGLR/JSASS International Electric Propulsion Conference, Colorado Springs, CO, May 11-13, 1987; revision received April 23, 1989.

*Director, Space Applications; currently Associate Professor, University of Illinois, Department of Aeronautical and Astronautical Engineering. Member AIAA.
†Senior Scientist.
‡Executive Vice President.
§President.

pulse. The standard technique used here for supplying low-energy, short-duration pulses is the capacitive pulse-forming network (PFN). The capacitors used in this investigation are 2-μF, 8-kV units designed for repetitive operation at up to 25 pps before overheating. The Princeton Circuit Analysis Program (PCAP) code[8] prediction for a 2-2-4 capacitor arrangement with 0.4-μH inductors was tried and proved successful. The 2-2-4 PFN and the resulting current pulse are shown in Figs. 3 and 4. The pulse width at half-maximum is 12 μs, and peak current is several kiloamperes.

As shown in Fig. 3, the PFN is electrically coupled directly to the PET thruster. The power supply is regulated for constant current, producing a capacitor voltage rising linearly with time until breakdown voltage is reached and the pulse begins (Fig. 5). The total energy discharged depends on the breakdown voltage, which varies somewhat from shot to shot as shown in Fig. 5. The variation is small enough, however, that the thrust is nearly constant when averaged over a few tens of pulses. This is indicated in the thrust stand response curves of Fig. 5.

The experiments were conducted in a steel vacuum tank with a volume of 1 m^3. The tank can be pumped down with a roughing pump to less than 1 Torr. With propellant flowing the pump cannot keep up, and the background pressure is 10–20 Torr, as determined by the vapor pressure of the water. Unfortunately, this rather high pressure precludes measurement of the exhaust velocity by time-of-flight techniques, as discussed later in the paper.

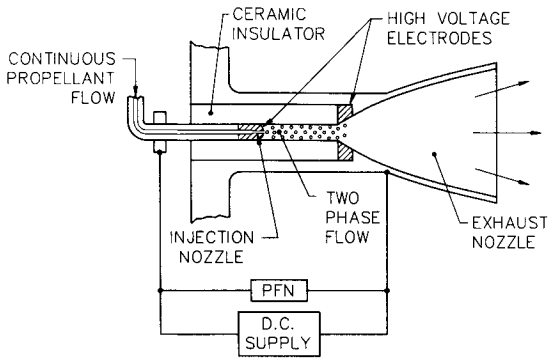

Fig. 2 Schematic of liquid-propellant PET thruster, with continuous water injection and pulsed electrical power supply.

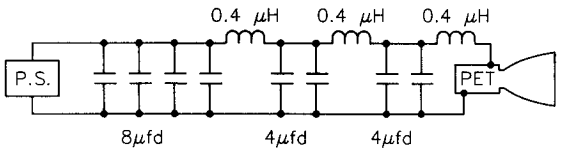

Fig. 3 Schematic of three-section 2-2-4 pulse-forming network, charged with a dc power supply and directly coupled to the thruster. The PFN, with an impedance of 0.31 Ω, produces 12-μs pulses.

Diagnostics for PET thruster performance measurements are the same as those reported previously.[2-4] The current is measured by a passively integrated Rogowski coil. Voltage is measured by a calibrated 1000:1 Tektronics probe. PFN capacitance is checked on a bridge, and when the current is time-integrated, agrees with the charge on the bank. Thrust impulse is detected on a thrust stand, which is calibrated with an impact calibration pendulum[4] whose velocity is measured to within 0.8% by detecting a focused laser passing through a Ronchi ruling mounted on the pendulum. The stand is operated with the axis vertical and is relatively friction free, typically executing five half-cycles before damping out. Each impulse causes the thruster mass, which is mounted on a ball-type linear bearing, to recoil at an initial velocity of a few mm/s. The recoil motion is detected with an inductive transducer (Bently-Nevada 7200 series Proximitor), which produces a highly linear output of 8.00 V/mm when opposed at a distance of 0–2 mm from the manufacturer-recommended AISI 4140 steel target, as is done here. The position-time (x-t) transducer signal is differentiated graphically to give the recoil velocity of the thruster, which when multiplied by the thruster mass gives the impulse bit for the pusle. Total thrust is then the average impulse bit (Newton-seconds) multiplied by the pulse rate. The thrust stand is calibrated by the impact calibration pendulum to within 2.0%.[4]

Previous single-shot PET thruster measurements[2-4] were taken at the 2000-J/pulse level and resulted in a high thrust stand signal-to-noise ratio. For repetitive operation only tens of joules were available for the discharge, and thrust stand signal-to-noise ratio was of some concern. Fortunately, the thrust stand design is capable of operating at two orders of magnitude less signal, although a small noise signal in the megahertz range is induced by the inductive transducer. This signal is of sufficiently higher frequency than that of the thrust stand natural frequency (20 Hz) that it is easily filtered out with a 0.05-μF capacitor across the Proximitor output.

The primary design problem for repetitive operation is the water injection nozzle, which is a 0.34-mm-diam × 1.0-mm-long orifice located inside the anode at the entrance to the 2.5-mm-diam discharge capillary (Fig. 6). For a typical discharge energy of 50 J and water enthalpy of 160 J/mg, the water mass requirement is 0.31 mg/pulse, giving a mass flow of 3.1 mg/s at 50 W (10 pps). At this rate the fluid injection velocity is 35 mm/s, giving a fluid travel distance between pulses of 3.5 mm. This is considerably less than the capillary length of 28 mm, effectively containing the water within the discharge capillary during the pulse.

The difficulty with injecting through an orifice or nozzle at low flow rates is drop formation caused by the water surface tension. A drop forms, breaks off from the nozzle tip, and fills the discharge capillary, causing erratic thruster breakdown. The solution used for these experiments is to overfeed the water mass flow rate sufficiently to form a constant-diameter axial jet. The estimated experimental flow rate is 820 mg/s, 266 times the ideal flow. In more recent experiments, PET thrusters have been operated at or very close to the ideal flow.

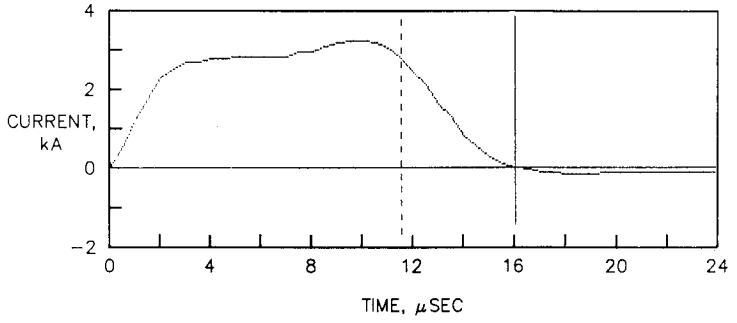

Fig. 4 Current pulse produced by the 2-2-4 PFN.

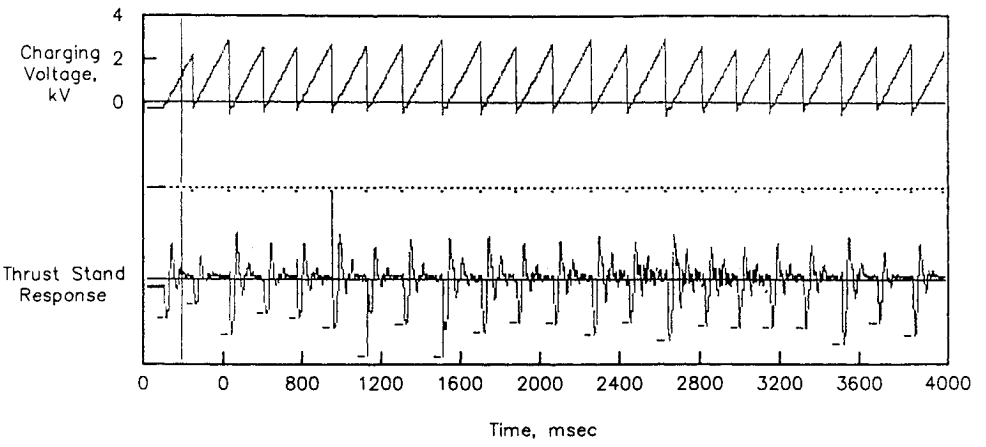

Fig. 5 Typical PET thruster run, showing the shot-to-shot variation in the charging voltage and thrust stand response.

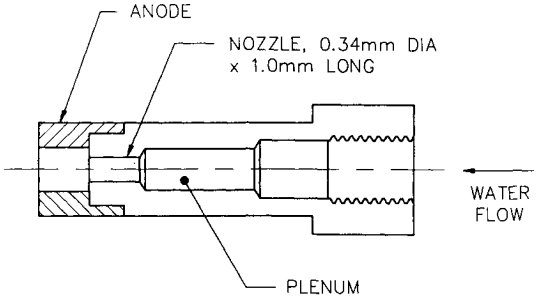

Fig. 6 Water injection nozzle, coupled to the anode.

Discharge-Fluid Coupling

Because of the small size of the discharge capillary, it is not possible to observe directly the dynamics of the waterjet during the discharge pulse. Prior to the pulse the injected water Reynolds number is 20,000; hence, the jet is presumed to be turbulent and breaking up into drops. As the pulse begins the discharge power increases to several megawatts in a few microseconds, heating the water vapor surrounding the jet and driving it toward the throat to a sonic velocity of about 6 km/s. At the same time, the capillary pressure increases to a few hundred atmospheres with a strong axial gradient and resulting high-velocity axial flow, and the temperature increases to 20,000 K, producing a blackbody radiation flux on the order of 2 MW/cm^2. It might be presumed that under these harsh conditions the jet would not maintain its integrity and would break into fine drops. The experimental evidence suggests that this is indeed the case, as discussed in the next paragraph.

A simple calculation shows that the water mass flow rate is not significantly interrupted by the discharge at repetition rates of less than 1000 pps. The water injection nozzle is 1 mm long and is connected to a plenum (Fig. 6). During the discharge the pressure rises to several hundred atmospheres, which slows the momentum of the incoming water. After the pulse the plasma pressure drops to tank ambient pressure in a few acoustic transit times, here about 10 μs. It takes about one acoustic time through the 1-mm-long liquid column in the nozzle, at a water sound velocity of 1500 m/s, for the pressurized plenum to sense that the discharge is over. This time, which is less than 1 μs, is so short that even at 1000 pps the injection flow has time to recover and is essentially undisturbed by the previous discharge pulse.

III. PET Thruster Measured Performance

The PET thruster performance is documented for a total of seven runs (runs 11–17) and is summarized in Table 1. These runs were performed without changing the thruster hardware, using the injector electrode nozzle shown in Fig. 6.

Table 1 PET thruster performance runs

Run	11	12	13	14	15	16	17	
Charging current, mA	73	73	73	490	490	270	340	
Repetition rate, pps	2	2	2	9	10	6	9	
Pulse energy, J	40	50	50	70	60	50	50	
Average power, W	80	100	100	630	600	360	450	
Total test pulses	200	100	100	4	4	300	300	=1000
Total test energy, J	8	5	5	0	0	12	15	=45

Runs 11–13 are at relatively low power (100 W). Runs 14 and 15 are maximum power (600 W), but overload the 500-W power supply, causing premature shutdown. Runs 16 and 17 are at a slightly reduced level of 400 W.

Three channels of data are recorded for each run: discharge voltage, discharge current, and thrust stand response. Data are recorded digitally on a Soltec signal memory recorder at two different sample rates: 2 MHz and 2 kHz. The scope is triggered on the falling signal from the thruster discharge voltage at the initial breakdown. The scope captures 2000 data samples before triggering, followed by 3000 data samples after triggering at the 2-MHz rate, which provides good time resolution for the voltage and current history of the first pulse. The scope then captures 11,000 points (5.5 s) worth of data at the slower 2-kHz rate, resolving the charging voltage and thrust stand response for several consecutive pulses. A typical run is shown in Fig. 7.

The discharge voltage and current time histories for the first pulse are shown for runs 11–13 in Fig. 8. The zero-to-zero current pulse length is 16 μs, and the full-width half-maximum (FWHM) length is 12 μs. The dc voltage level at negative time gives the bank charging voltage (2112–2560 V). The product of V and I when integrated over the pulse gives the energy transferred to the discharge, which is 99% of the initial stored energy. The remaining 1% of the stored energy is lost as resistive heating in the external circuit.

A typical voltage, current, and thrust stand response is shown in Fig. 7 for run 11. The repeatability of the discharge voltage can be observed in each case. The discharge voltage is observed to fall from an initial value of 2100 V to a negative value of a few hundred volts. This is a consequence of the thruster being directly attached to the capacitor bank. When the discharge power is insufficient to ionize the water, the thruster stops conducting and the current stops flowing. The discharge current is never observed to reverse, and the pulse always ends with a small reverse voltage on the bank. This reverse voltage is small enough that the remaining PFN energy is negligible, and the cycle life of the 8-kV capacitors is not adversely affected.

The initial slope of the thrust stand x-t response is an exact measure of the recoil velocity, and hence impulse bit, but the amplitude of the first negative peak is a more readily visualized indicator of this velocity. These amplitudes and their shot-to-

shot variation can be observed in Fig. 7. It should be noted that the mean value of thrust holds relatively constant when averaged over any 10 consecutive discharges.

Data Analysis

The thrust-to-power ratio is

$$\frac{T}{P} = \frac{\int T\,dt}{\int P\,dt} = \frac{\text{impulse bit}}{\text{stored energy}}$$

The impulse bit is measured by the thrust stand, and the stored energy is measured by the capacitance and bank voltage. It is more correct to define T/P as impulse bit/delivered energy, but delivered energy and stored energy are nearly equal, as was discussed earlier. Values of T/P for the first pulse in each run are shown in Table 2. This table gives a mean T/P of 0.073 N/kW for runs 11–17. The power level in these runs is varied from 100 to 600 W by varying only the pulse rate and not the energy of an individual pulse; thus, it is meaningful to compare T/P at different power levels.

Discussion of Data

In Fig. 8, the time range from 3 to 11 μs is referred to as the flattop region, where the voltage and current vary relatively slowly. It can be seen (Fig. 8) that the voltage-to-current ratio is nearly constant in the flattop region; hence, resistance and therefore plasma temperature change very little.

The experimental observation of constant resistance had not been expected, since it had been assumed that the resistance would fall continuously during the pulse as the water vapor plasma was heated. It can also be seen (Table 2) that the resistance value (measured at $t = 5$ μs) is relatively constant at $V/I = 0.40$ Ω, despite a factor-of-two variation in the discharge power from 3.1 to 6.2 MW. This constant resistance/constant discharge temperature behavior is probably a consequence of two-phase flow.

The model that best fits this data is one in which the liquid jet breaks into droplets, which then continuously evaporate to replace the heated vapor exiting from the throat. The data imply that the jet must break up, since the surface area of the water would otherwise be too small to capture the discharge radiation before it reaches the capillary wall and is lost, cutting the evaporation rate and roughly doubling the temperature. A third possibility, in which the liquid converts quickly to a fine mist or vapor, would imply a continuously rising temperature and dropping resistance, which is not observed.

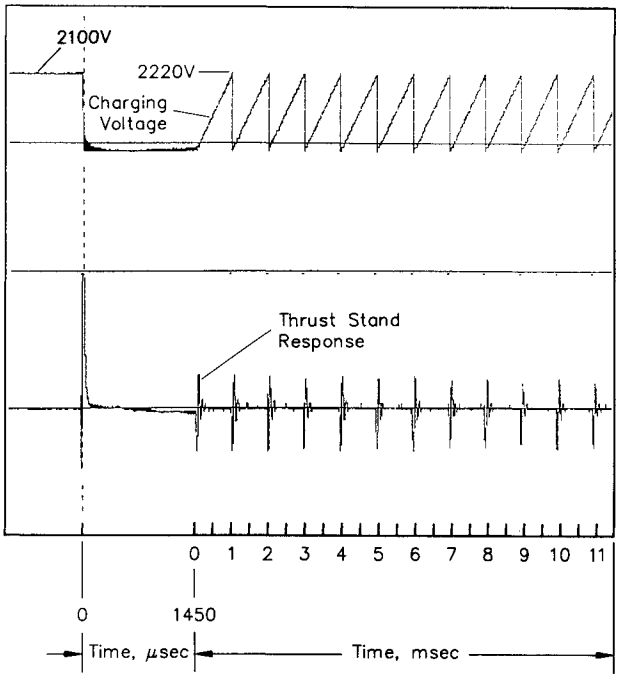

Fig. 7 Charging voltage and thrust stand response data for run 11, showing the two sweep rates used to acquire data from the first pulse and then from the pulse train.

Discharge Model

Discharge conditions are calculated from a volume-averaged steady-state electrical/flow model,[9,10] which assumes Spitzer resistivity, corrected for electron-neutral collisions, and a bal-

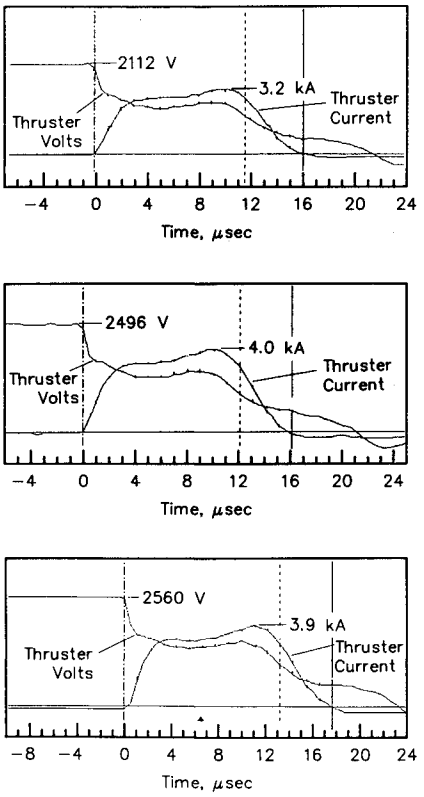

Fig. 8 Discharge voltage and current time histories for three runs at 2-pps repetition rate: run 11 (top); run 12 (middle); run 13 (bottom).

Table 2 Samples of data from runs 11–17

Run	11	12	13	14	15	16	17
Impulse bit, mN-s	2.8	4.2	4.1	5.4	3.6	3.8	2.8
$CV_0^2/2$, J	35	50	52	68	58	58	51
Thrust/power, N/kW	0.079	0.083	0.077	0.079	0.063	0.065	0.062
Discharge resistance, Ω	0.40	0.41	0.44	0.39	0.41	0.38	0.38
Power IV, MW	3.1	4.5	4.9	6.2	4.9	5.4	4.1

Table 3 Calculated properties of discharge from model and comparison with experiment

	Run 11	Run 12	Run 13	Run 14
PFN impedance, Ω	0.31	0.31	0.31	0.31
Source voltage, kV	2.11	2.50	2.56	2.91
Plasma specific heat ratio	1.20	1.20	1.20	1.20
Discharge current, kA	2.95	3.44	3.39	4.12
Resistance, Ω	0.40	0.41	0.44	0.39
Temperature, eV	1.74	1.71	1.64	1.78
Sound speed c_0, km/s	5.80	5.80	5.70	6.00
Stagnation pressure p_0, atm	280	400	420	520
Calculated impulse bit, mN-s ($C_F = T/p_0A_t = 1.7$)	2.8	4.1	4.3	5.3
Measured impulse bit, mN-s	2.8	4.2	4.1	5.4

Table 4 PET thruster performance

	Run 11	Run 12	Run 13	Run 14
Calculated temperature, eV	1.74	1.71	1.64	1.78
Calculated enthalpy, J/mg	171	168	161	175
Discharge energy, J	35	50	54	68
Exhaust mass, mg	0.20	0.30	0.34	0.39
Measured T/P, mN-s	2.8	4.2	4.1	5.4
Exhaust velocity, km/s	14	14	12	14
Efficiency, $U_e(T/P)/2$	0.55	0.58	0.46	0.55

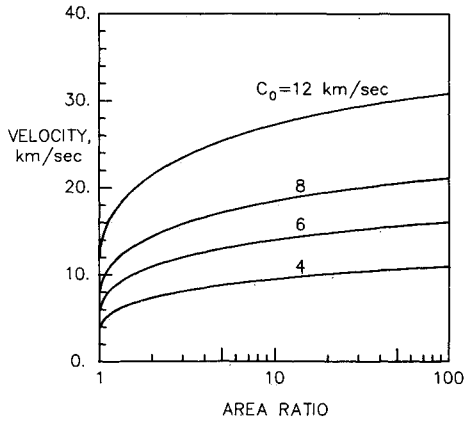

Fig. 9 Plasma exhaust velocity based on equilibrium flow and real chemistry for four values of the stagnation sound speed as a function of nozzle area ratio.

ance between radiation flux, evaporated water enthalpy flux, and nozzle enthalpy flux. The discharge is driven in the model by a constant-impedance PFN.

Because of the high plasma density (10^{20}–10^{21}/cm^3) and a pulse length of 12 μs, use of an equilibrium flow model is justified. Thermal equilibrium exists well into the nozzle and breaks down only when the molecular recombination time exceeds the nozzle flow time. From the model of Zel'dovich and Raizer,[11] the characteristic recombination time is

$$t_r = (2\sigma \bar{v} V_{H_2O} n_H^2)^{-1}$$

where

σ = H-OH scattering cross section, cm^2

$\bar{v}$ = mean thermal velocity, $(8kT/\pi m_H)^{1/2}$, cm/s

V_{H_2O} = volume of water molecule, cm^3

n_H = atomic species density, cm^{-3}

For $\sigma = 10 \times 10^{-16}$ cm^2, $\bar{v} = 1.5 \times 10^6$ cm/s at 1 eV (11,600 K), $V_{H_2O} = 1.3 \times 10^{-23}$ cm^3, and $n_H = 2 \times 10^{18}$ cm^{-3} at 4 atm and 1 eV, the recombination time is 6 μs. During this time water vapor particles flowing through the nozzle move about 6 mm, which is a small percentage of the nozzle length. When the density drops further as the particles expand, the recombination time exceeds flow time and the chemistry is frozen, preventing further recovery.

The steady-state assumption requires that acoustic travel time in the capillary be less than pulse length. With a sound speed of $c = 6 \times 10^5$ cm/s and a capillary length $L = 3$ cm, the acoustic time is $L/c = 5$ μs, justifying the steady-state assumption for the 12-μs pulse.

The steady-state discharge model predicts the temperature. Stagnation sound speed and specific heat ratio are then interpolated from the Los Alamos Sesame tables.[12] The results are shown in Table 3 for runs 11–14.

At the bottom of Table 3 are listed the calculated and measured impulse bits. The calculated impulse bit $\int T\,dt$ is written

Table 5 Tungsten alloy erosion measurements for 1400 shots

	Throat electrode	Injector electrode
ID increase, mm	0.00	0.00
OD decrease, mm	—	0.00
Length decrease, mm	0.00	0.15
Total mass loss, mg	0.00	28.0
Mass loss/pulse, μg	0.00	20.0

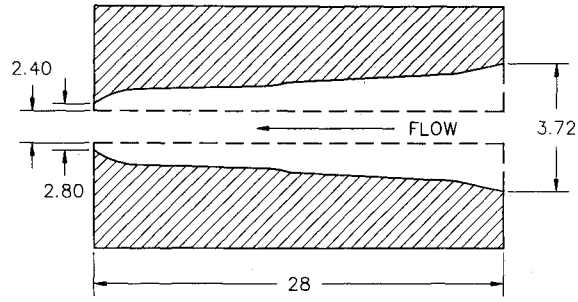

Fig. 10 Measured ablation of the boron nitride insulator, showing higher ablation at the closed end due to radiation (right) than at the open end (left).

as the product of thrust coefficient C_F, calculated stagnation pressure p_0, throat area A_t, and pulse length t_p, which is taken as the half-maximum pulse length of 12 μs:

$$\int T\,dt = C_F(p_e/p_0, A_e/A_t, \gamma) p_0 A_t t_p$$

In this equation C_F is a function of the pressure, area ratio, and specific heat ratio; the C_F equation for steady flow is given in Ref. 13. C_F is not well known for the present case of impulsive flow in a nozzle containing an ambient fill, but is probably between 1.2 for the case of no nozzle and about 2.0 for a 1000:1 nozzle. A value of $C_F = 1.7$ is adopted for Table 3, which then gives calculated impulse bits very close to the measured values. Considering the approximations made, this agreement is reasonable and provides experimental evidence that the calculated values of pressure and temperature are close to those occurring in the discharge chamber.

Performance

Because of the high ambient background pressure in the tank, the exhaust velocity must be estimated, rather than measured from time of flight as was done previously.[2-4] Estimation of the velocity is done from the measured energy per pulse, calculated enthalpy, and measured impulse bit. From the average calculated temperature of 1.71 ± 0.07 eV in Table 3, the enthalpy from the Sesame tables[12] is 168 J/mg. For runs 11–14 where the discharge pulse energy is measured, we can calculate an exhaust velocity, as shown in Table 4.

The estimated exhaust velocity is about 14 km/s, which gives a specific impulse of 1400 for 100% mass utilization. The estimated uncertainty in the exhaust velocity is 15%: 5% from the impulse bit measurement and 10% from the calculated exhaust mass.

The conversion efficiency from electric to kinetic energy is given by

$$\eta = U_e(T/P)/2$$

where T/P is given in Table 2 and U_e is from Table 4. The efficiency values range from 0.46 to 0.58 with a mean value of 0.54, as shown in Table 4.

The plasma exhaust velocity can also be derived from the sound speed and the nozzle expansion ratio. A steady-state adiabatic nozzle flow model, which includes the variation in the specific heat ratio, has been developed,[14] and the predicted velocity for water as a function of area ratio is shown in Fig. 9. The curve for $c_0 = 6$ km/s shows that an expansion ratio of

only 10 is required to achieve 14 km/s. For a lower background pressure where the effective area ratio is 1000, the expected exhaust velocity increases from 14 to 17 km/s, and the mean efficiency increases from 0.54 to 0.66.

Propellant Utilization

The effect of propellant overfeeding on performance is evaluated by assuming that the flow is two phase and that only the vapor phase participates in the discharge and nozzle expansion process. The liquid phase is seen as a mass reservoir, the surface of which is evaporated to produce the pulse mass requirement, as determined by the pulse energy and temperature. The principal effect of overfeeding is therefore to reduce specific impulse, in inverse proportion to the amount of overfeeding. The excess liquid does not participate in the discharge and exits the exhaust nozzle at nearly the same low velocity at which it was injected.

Ablation

The PET thruster must ultimately operate in an ablation-free mode, so that total impulses of 2×10^5 to 2×10^7 N-s, requiring 5×10^7 to 5×10^9 pulses, can be achieved. It is found on the present experiments that ablation is relatively high, as determined by mass and dimensional measurements. The thruster is subjected to a number of pulses of varying energies, with an estimate of 1400 for total number of pulses. The least ablation is experienced by the tungsten alloy electrodes and the most by the boron nitride insulator.

Tungsten electrodes are located at the throat and 28 mm back at the injection orifice. Tungsten erosion is summarized in Table 5. We see that the throat electrode has no measurable erosion, probably because the throat is cooler than the stagnation region at the injector electrode. The 0.020-mg/shot loss from the injector electrode is caused by less than 0.1 J/pulse being converted to hot tungsten. The total calculated radiated energy is about 1.0 J/pulse, or 10 times the amount required to cause ablation; thus, the mass loss must occur at the tail end of the pulse. A slightly shorter pulse or cooler discharge would have prevented ablation of this electrode altogether. The throat never does reach the melting point, according to the data.

Ablation of the boron nitride insulator follows a pattern consistent with the electrodes, in that more ablation occurs at the injector end than at the throat end. This implies a predominantly radiative heat-transfer mechanism. If the ablation were caused by convective heat transfer rather than radiation, the reverse would be true and the throat would ablate more. However, maximum convective heat transfer at the throat is calculated to be only 0.2 MW/cm^2, or 40% of the radiative contribution.

The insulator ablation is shown in Fig. 10. The mean radial ablation is 0.36 mm, and the total mass loss is 180 mg, or 0.12 mg/shot. The enthalpy of the evaporated boron nitride is about 50 J/mg; hence, the energy absorbed by the insulator is 6 J (12 mg/shot $\times$ 50 J/mg), equal to 10% of the mean total of 60 J in the discharge. The remaining 90% is absorbed by the water propellant.

IV. Summary and Conclusions

Preliminary performance measurements have been accomplished with a repetitive PET thruster using water propellant. Operating at an overfed condition to produce an injection jet, the thruster T/P is 0.07 N/kW. Temperature estimates based on discharge resistance indicate a plasma velocity of 14 km/s. This is to be compared to previous results with an ablative polyethylene wall thruster, which gave 15–17.5 km/s[3]. It is suggested that the present performance would improve significantly with a lower background pressure in the test tank.

The principal reason that performance is high with water injection is the reduced temperature of the discharge. The previous work with polyethylene was performed at 2.5 eV (29,000 K), whereas the present thruster is operated at 1.7 eV (20,000 K) and a comparable pressure. The recovery of dissociation energy with water is therefore more complete, leading to better performance.

Despite the lower temperature and use of water injection, some ablation of the injector electrode and insulator occurs. Comparison of the ablated mass with the wall energy flux suggests that the energy flux needs to be reduced 10–20% per pulse to eliminate ablation caused by radiative melting of the surface. This can be accomplished with straightforward changes in the thruster geometry.

This work has demonstrated technical feasibility for the water-propellant PET thruster at 1000–2000 s. Because liquid water injection is easier to accomplish at higher mass flow rates, applications of the PET thruster would seem to lean toward mean power levels above 5 kW.

Acknowledgments

This work was supported in part by NASA Lewis Research Center Contract NAS 3-24636 and in part by GT-Devices. We are grateful to Thom Chichester of GT-Devices for many design and technical contributions and to Steve Brown for the final thruster design.

References

[1]Burton, R. L., Goldstein, S. A., Tidman, D. A., and Winsor, N. K., "Theory of the Pulsed Electrothermal Thruster," AIAA Paper 82-1952, Nov. 1982.

[2]Burton, R. L., Goldstein, S. A., Hilko, B. K., Tidman, D. A., and Winsor, N. K., "Investigation of a Pulsed Electrothermal Thruster," GT-Devices, Alexandria, VA, NASA CR-168266, Oct. 1983.

[3]Burton, R. L., Goldstein, S. A., Hilko, B. K., Tidman, D. A., and Winsor, N. K., "Experimental Investigation of the Pulsed Electrothermal (PET) Thruster," AIAA Paper 84-1386, June 1984.

[4]Burton, R. L., Goldstein, S. A., Hilko, B. K., Tidman, D. A., and Winsor, N. K., "Investigation of a Pulsed Electrothermal Thruster System," GT-Devices, Alexandria, VA, NASA CR-174768, Oct. 1984.

[5]Burton, R. L., Goldstein, S. A., Hilko, B. K., Tidman, D. A., and Winsor, N. K., "Proposed System Design for a 20 kW Pulsed Electrothermal Thruster," AIAA Paper 84-1387, June 1984.

[6]Burton, R. L., et al., U.S. Patent Application No. 743,150, *Pulsed Electrothermal Thruster,* June 10, 1985.

[7]Burton, R. L., Fleischer, D., Goldstein, S. A., Tidman, D. A., and Winsor, N. K., "Investigation of a Repetitive Pulsed Electrothermal Thruster," GT-Devices, Alexandria, VA, NASA CR-179464, Aug. 1986.

[8]*Princeton Circuit Analysis Program,* Princeton University, Department of Electrical Engineering, Princeton, NJ 08540.

[9]Tidman, D. A. and Goldstein, S. A., "Thermal Transport to Hypervelocity Gun Tubes by High Pressure Partially Ionized Gas Flows," GT-Devices, Alexandria, VA, TN GTD 85-4, May 1985.

[10]Tidman, D. A., Thio, Y. C., Goldstein, S. A., and Spicer, D. S., "High Velocity Electrothermal Mass Launchers," GT-Devices, Alexandria, VA, TN GTD 86-7, Sept. 1986.

[11]Zel'dovich, Ya. B., and Raizer, Yu. P., "Atom Recombination Rates and Dissociation Rates for Diatomic Molecules," *Physics of Shock Waves and High-Temperature Hydrodynamic Phenomena,* Vol. I, Academic, New York, 1966, pp. 364–368.

[12]SESAME Equation of State Library, Los Alamos Scientific Lab., Los Alamos, NM, Rept. LASL-79-62, 1979.

[13]Shapiro, A. H., "Thrust of Rocket Motor," *The Dynamics and Thermodynamics of Compressible Fluid Flow,* Vol. I, Ronald Press Co., New York, 1953, pp. 101–103.

[14]Hubbard, R. F., Slinker, S. P., Tidman, D. A., Winsor, N. K., Burton, R. L., and Goldstein, S. A., "Steady State Nozzle Flow Model for Sound Speed Dependent γ," GT-Devices, Alexandria, VA, TN GTD 85-1, Jan. 1985.